# A BORESCOPE DESIGN TOOL FOR LASER MEASUREMENTS IN FLUIDS


**Carvalho Figueiredo, A.J.** ajcbsd20@bath.ac.uk

**Jones, R. R.** R.R.Jones@bath.ac.uk

**Sangan, C.M.** C.M.Sangan@bath.ac.uk

**Cleaver, D.J.**[1] D.J.Cleaver@bath.ac.uk

Department of Mechanical Engineering
University of Bath
Bath, BA2 7AY
United Kingdom



## ABSTRACT

This paper presents the method, implementation and validation of a borescope probe design tool devised for the challenges of optical fluid measurement techniques. The design tool is capable of predicting the path and power distribution of the laser beam through the probe and into the region interest, ensuring a cost and time-efficient design process that removes the need for experimental trials. The associated code is available as supplementary material.

Optical measurement techniques have become established methods within fluid dynamics research. In contrast, their application to turbomachinery rigs is usually limited due to the restricted optical access. A small number of studies have circumvented this problem by employing borescopes to introduce the laser beam into the measurement region but wider application is inhibited because these probes are difficult to design, expensive and usually require several iterations until a suitable design is achieved.

The first part of the paper presents the structure of the software program and the mathematical modelling of the optics for predicting the beam path into the measurement region. The second part presents different design options and the manufacture of a typical probe with validation in a wind tunnel facility using volumetric velocimetry. The borescope results agree very well with measurements acquired using direct illumination through a window demonstrating the efficacy of the method.



**Keywords:** Borescope, laser beam delivery, volumetric velocimetry, optics modelling, turbomachinery



[1] corresponding author


## 1 INTRODUCTION

Optical fluid measurement techniques such as Particle Image Velocimetry (PIV), Planar Laser Induced Fluorescence (PLIF), and Volumetric Velocimetry (VV), are becoming increasingly popular for fluid dynamics research because they offer several advantages over traditional methods, primarily they are non-intrusive, capture a wide spatial region and are efficient. The capability of optical fluid measurement techniques, in particular velocimetry techniques, is very relevant to turbomachinery research due to the highly complex three-dimensional flows. However, these techniques are not commonly used due to the challenges of beam delivery and image acquisition inside turbomachinery. For stationary rigs PIV can now be considered an established technique where rotating rigs present a more challenging environment. The number of studies using optical techniques is therefore very limited. A review on the applications of PIV to turbomachinery rigs can be found in Woisetschläger and Göttlich [1]. The primary obstacle to greater uptake of optical measurement techniques in turbomachinery is solving the challenge of optical access in a practical and flexible manner.


**Declarations of interest**: none.


**Abbreviations**

| | |
|---|---|
| CS | control surface |
| DR | density ratio |
| IR | momentum flux ratio |
| PDA | Power Density Average |
| PDM | Power Density Maximum |

**Table 1: Comparison of borescope probes.**

| *Study* | *Experimental Technique* | *Collimated Beam* | *Beam Shaping Optics* | | | *Cover Window* | *Local Enclosure* |
|---|---|---|---|---|---|---|---|
| | | | *Cylindrical Lens* | *Spherical Lens* | *Mirror or Prism* | | |
| **[2]** | PIV | yes | 1 | - | Prism | - | - |
| **[3]** | S-PIV | yes | 1 | - | Prism | - | - |
| **[4]** | S-PIV | yes | 1 | 1 | - | - | - |
| **[5]** | PIV | no | 1 | 1 | Mirror | 1 | - |
| **[6]** | PIV | yes | 1 | 1 | Prism | - | Wake Generator |
| **[7]** | PIV | yes | 1 | - | Mirror | - | Turbulence Bar |
| **[8]** | PIV | yes | 2 | - | Mirror | - | Vane |

Several solutions for the optical access problem can be found in the literature, including a few unconventional methods. For instance, Geis *et al.* [9] employed an endoscope to provide optical access for the camera and a window to introduce the laser beam. Kegalj and Schiffer [10] also used a probe for the camera access, this time coupled with a second probe for laser delivery. Chow *et al.* [11] employed a turbomachine with an acrylic rotor and stator and used a solution with a refraction index equal to acrylic as the working fluid, thus making the vanes and blades transparent to the laser beam. Optical access for the cameras was provided by a window. Besides these novel approaches, the most common approach is to introduce the laser beam through a borescope and to use a window embedded in the casing for the camera. In most designs, the borescope is composed of one or two lenses for shaping the beam and a reflective surface to reflect the laser beam 90 degrees into the measurement region. This may be preceded by collimating or beam-limiting lenses and followed by a protective window or a local enclosure.

A selection of several studies that employed borescope probes is presented in Table 1. Several other names are used to describe borescopes: endoscopes, periscopes or light sheet probes are the most common. When discussing the following studies these devices are simply referred to as probes. Balzani *et al.* [2] studied the blade-to-blade flow in a compressor rotor using PIV with a probe that contained a cylindrical lens to generate a laser sheet and a prism to reflect the beam 90 degrees. The beam was collimated before travelling down the probe axis. The probe was inserted upstream of the measurement location in the compressor rig, but moved longitudinally in order to ensure that the wake of the probe did not interfere with the flow in the measurement region. A similar design was employed by Göttlich *et al.* [3] in a transonic turbine. This study employed a Stereo-Particle Image Velocimetry (S-PIV) system, delivering three components of velocity in the plane of measurement. Liu *et al.* [4] also employed S-PIV with the measurements performed on a laser sheet perpendicular to the vane exit angle. The probe was placed between the two cameras in an arrangement that did not require a mirror to reflect the beam 90 degrees. The beam shaping optics were composed of a cylindrical lens and a spherical lens. Wernet [5] employed a laser sheet probe with similar beam shaping optics in a compressor rig in order to conduct PIV measurements. After the beam shaping optics the beam is turned 90 degrees with a mirror and finally travels through a window that protects the optics inside the probe.

References [6-8] (see Table 1) exploit the geometry of the test rigs to introduce the laser beam for PIV studies. Instead of placing the probe in the flow, the probe is introduced (or built) using geometry already existent in the test rig, therefore reducing or completely avoiding any probe-induced flow disturbance. Copenhaver *et al.* [6] used a modified wake generator to insert the laser beam. The beam was introduced radially and was first reflected into the axial direction by a prism inside the wake generator and then shaped into a sheet by a cylindrical and a spherical lens. A further prism reflected the beam 90 degrees, delivering a laser sheet perpendicular to the radial direction. The probe was placed far from the measurement region since a small part of the probe protruded from the wake generator.

Bryanston-Cross *et al.* [7] used a turbulence bar to introduce the laser beam into a transonic annular turbine cascade. The turbulence bar was fitted with a mirror and a cylindrical lens to deliver a laser sheet for PIV measurements. Unlike other studies, the mirror was placed at an angle different from 45 degrees in order to deflect the beam at an angle equal to that of the casing wall. Also in contrast with most previous studies, the cylindrical lens was placed after the reflective surface.

Chana *et al.* [8] used vanes fitted with optical windows to introduce the laser beam into a transonic turbine stage. Two cylindrical lens and a mirror delivered a laser sheet perpendicular to the radial direction. Two probes (inside two vanes) were employed in order to cover the measurement region. Since the probes were fitted inside windowed vanes they caused no flow disturbance.

The different probe designs presented in the literature show the need for bespoke designs for every application. However, currently no standard design guidelines are available even though the probe design is crucial to the application of these experimental techniques.

*Objectives*

The main aim of this study is to develop a practical and flexible optical design tool for borescope probes applicable to fluid measurement techniques. Three objectives are defined in order to achieve this aim: (i) development of the design tool, (ii) design and manufacture of an example probe and (iii) validation of the probe through volumetric velocimetry measurements.

## 2 Design Tool Architecture

The design tool predicts the laser beam path through the computation of the refraction or reflection of the beam at several control surfaces (CSs). Its structure and optics are

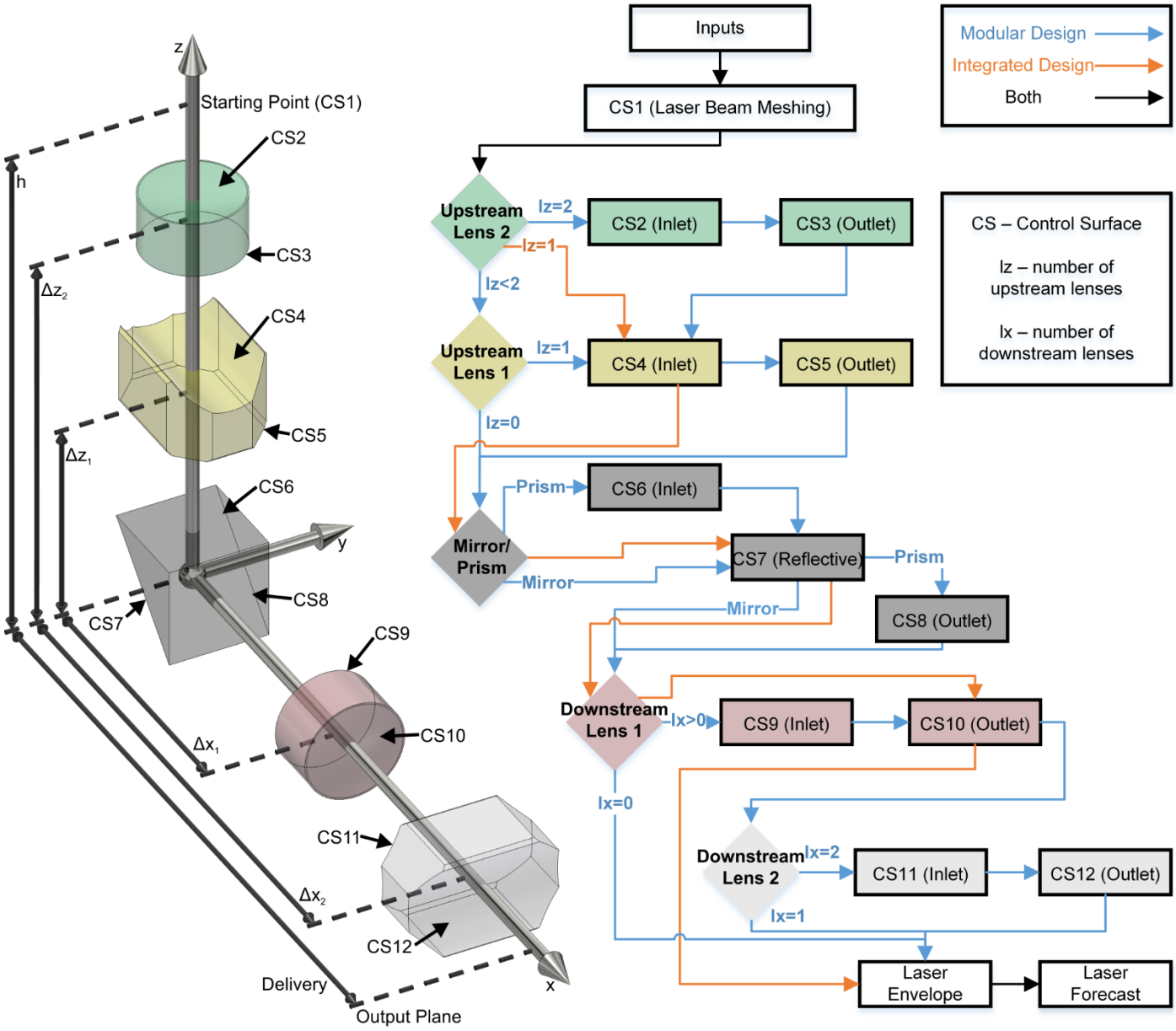


**Figure 1: Control surfaces in the MATLAB program (left) and flow chart of the Borescope MATLAB program (right).**

informed by the most common designs for laser sheet probes. It can be used to design probes for diverse applications, *e.g.* to deliver a laser sheet or illuminate a region with a laser cone. This enables the application of these probes to PIV and Planar Laser-Induced Fluorescence (PLIF), which require a laser sheet and VV, which requires an illuminated volume, *i.e.* a laser cone. Finally, since the main purpose of the application is deployment in turbomachinery rigs, the program is also capable of computing the path of the laser beam through a local enclosure defined by a set of coordinates. This can be a vane, a turbulence bar or any other geometry that can be defined by a set of coordinates given to the software.

Its architecture is divided into four parts: inputs, discretization of the laser beam, computation of the beam path at different control surfaces and plotting. Figure 1 shows the lens combinations that can be modelled (left) and a flowchart of the process (right). The plots of the output laser power distribution at the end are essential for evaluating the borescope design.

Two general types of borescope designs are considered: modular and integrated. A modular design is composed of several distinct lenses whilst an integrated borescope is composed of a single machined optical component. This design can be understood as a right-angle prism mirror with machined inlet and outlet surfaces.

For a modular borescope design (Figure 1 flowchart, blue connecting lines), the process begins with the user inputs, where a user can prepare a simulation of the laser path by choosing from an array of lens combinations and parameters. The beam is first discretized at the starting point, Control Surface 1 (CS1). After this, it encounters up to two (optional) lenses before being reflected at an angle (usually 90 degrees). These are denominated *upstream lenses* and comprise CS2 to CS5 (each lens has two CSs: inlet and outlet). The *reflection element* can be either a mirror or a prism. These are CS6 to CS8. The *downstream lenses* follow, representing CS9 to CS12. If the borescope is placed in an enclosure then two more CS are needed (CS13 and CS14): the inside surface

(assumed planar) and the outside surface of the enclosure, dictated by a set of coordinates given in the inputs. Finally, the coordinates of each beam ray are calculated at a user defined delivery distance, CS15, to define the laser envelope and its distribution.

An integrated borescope design is limited to one control surface upstream of the reflection (inlet surface of upstream lens 1) and one control surface downstream of the reflection (outlet surface of downstream lens 1). This design is displayed in the flowchart in Figure 1 (right) through orange connecting lines.

Both modular and integrated borescopes are possible with the design tool and have been implemented in a MATLAB code attached as supplementary material and referred to as the program. The following subsections explain each of the components that make up the architecture in more detail, including the inputs implemented in the program to make it as versatile as possible. The mathematical modelling is described in Section 3.

### 2.1 Structure Definition

The first stage is to define the structure of the borescope, *i.e.*, modular or integrated, the number of lenses, etc. In the program this is achieved through a series of toggle variables that define: (i) modular or integrated, (ii) number of upstream lenses (up to two), (iii) the number of downstream lenses (up to two), and (iv) include or exclude an enclosure (CS13 and CS14) defined by a set of points.

The lens material will have an index of refraction different to that of air. The refractive index $n$ is defined individually for each component of the borescope. This enables the simulation of a modular design borescope using different materials for each lens. Likewise, the transmissivity of each lens is defined by the user in the inputs. The transmissivity can be estimated according to the material and thickness of the lens.

### 2.2 Laser Beam Discretization

The input laser beam can be defined through several parameters. The most important is the beam diameter $D_{beam}$. In the program, the beam cross-section is a circle (default) or an ellipse. This can be converging or diverging, displaced from the geometric centre of the borescope, or angled with respect to the borescope $z$ axis. Sections of the beam cross-section can also be clipped by confining the window range in terms of $x$ and $y$.

Once its 2D cross-section is defined the laser beam is discretized into a mesh, composed of an array of $N_c$ concentric ellipses, with the last ellipse corresponding to the outer edge of the beam. Each ellipse is discretized into evenly spaced $N_p$ points. A point is added in the centre of the beam. The result is an array of $N_pN_c$+1 points. A vector in the form of a dummy point is calculated as a function of the position of the beam with respect to the borescope reference frame, and associated to each of these points, thus achieving a discretization of the laser beam into individual rays.

A laser power distribution is fitted to the discretized points in order to distinguish the regions of higher power in the centre from the outer edges where laser power density is lower. This is achieved by applying a top-hat distribution (built with two Gaussian functions) to the mesh and associating the value of laser power of each beam ray to a colour map. It is possible to change the shape of this distribution to account for different laser beam profiles. Figure 2 shows a comparison between the actual power distribution of the laser beam used in this study (supplied by the manufacturer – Quantel) and the power distribution employed in the program. This figure also presents the circular pattern of individual points that model the laser beam, as well as the top-hat distribution applied for this particular case (solid line). The core region (with higher power) is highlighted. The amount of laser power in each pulse is an input, used to compute the power and power density available at the output.

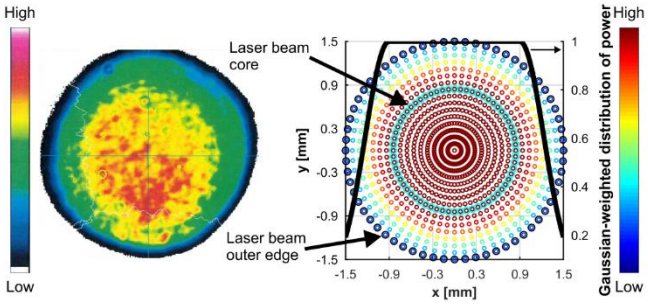


**Figure 2: Laser power distribution: measured beam profile (left) and simulated mesh (right).**

### 2.3 Upstream and Downstream Lenses

Several types of beam shaping lens can be simulated in the program. These include plano-cylindrical, bi-cylindrical, plano-spherical and bi-spherical lenses or a simple planar window. These lenses are defined by a radius, a centre thickness and a concave or convex toggle. For non-symmetrical lenses, such as plano-cylindrical or plano-spherical lenses, a further toggle defines the orientation of the lens. To define the location of the lens in 3D space and its interaction with the laser beam it is necessary to set: (i) the distance between the lens centre point and the origin of the reference frame (see Figure 1 (left)) and (ii) the useful area of the lens. Any beam ray outside the useful area of the lens is ignored in further calculations and that portion of the beam is marked as lost.

### 2.4 Reflective Element

Two types of reflective elements can typically be applied in borescopes: a prism or a mirror (only first surface mirrors are considered within the program). The prism is modelled in the program through three CSs. The mirror is modelled through a single reflective surface. Substrate coatings are common for both mirrors and reflective prisms. These coatings are taken into account through a toggle in the inputs.

Even though 45° planar reflective surfaces are the norm, other surfaces can also be machined, this is particularly true for integrated designs. As such, two more geometries can also be modelled in the program: a conical shape and a spherical shape.

### 2.5 Enclosure

So as to remain non-intrusive the borescope can be enclosed inside an internal geometry with transmission

through a window. Figure 3 shows an example implementation in turbomachinery where the borescope is embedded inside a vane. This example is similar to the application in [8]. The vane is static and has a transmissive window that refracts the laser beam at two CSs. The outer radius of the window is selected to approximate the profile of the vane's outer surface. The inner surface of the window is a simple planar surface. A detailed view of the beam refraction through the window is shown in Figure 3b. The resulting laser cone illuminates the flow downstream of the vane, primarily the axial gap between stator and rotor and the intra-blade passage of the rotor. The borescope can be rotated inside the vane in order to illuminate different regions of the downstream flow. The main challenge in applying optical techniques to turbomachinery is the restricted optical access. This configuration offers a viable solution for introducing a laser in a turbine or a compressor.

In the program, the location of the internal CS is defined with the $(x, y)$ coordinates of two points. The enclosure profile is read from a text file with $(x, y)$ coordinates and translated so that the origin of the enclosure coordinate system coincides with the location of the borescope axis within the enclosure (also an input). The $(x, y)$ coordinates of these surfaces are assumed to be valid for any *z*.

### 2.6 Outputs

When assessing the efficacy of a borescope the variables of interest are the total output power and how the beam is distributed spatially. In the program the spatial distribution of power is observed through a series of plots. The total output power depends on the user-defined input power and the user-defined Gaussian distribution. The volume (*V*) under a dome defined by the 3D Gaussian distribution of laser power is directly proportional to the beam power. If I is the group of i points in the beam mesh, with an assigned value *G* in the Gaussian-weighted power distribution, the total volume under a dome defined by the Gaussian distribution of the beam is given by Equation (1).

$$\boldsymbol{V_{beam} = \sum_{i=1}^{I} G_i A_i} \qquad \textbf{(1)}$$

where $A_i$ is the area surrounding (and unique) to each point. If the beam is clipped off at the input of the borescope, part of the beam is lost. The resulting group of points is denominated *J* ($J \supset I$). Similarly, after going through the borescope, parts of the beam may be lost, creating a smaller group of points that make up the resulting part of the beam at the output. This group is denominated *K* ($K \supset J \supset I$). Therefore, knowing the power of the beam $P_{beam}$, we may write Equations (2) and (3).

$$P^b_{input} = \frac{\sum_{j=1}^{J} G_j A_j}{\sum_{i=1}^{I} G_i A_i} P_{beam} \qquad \textbf{(2)}$$

$$P^b_{output} = \frac{\sum_{k=1}^{K} G_k A_k}{\sum_{i=1}^{I} G_i A_i} P_{beam} T_{rs} \qquad \textbf{(3)}$$

For $P^b_{output}$ it is necessary to take into account the overall transmissivity $T_{rs}$, a measure of the percentage of the power of the beam that is not lost in unwanted reflections throughout the borescope (for example when the beam enters a prism,

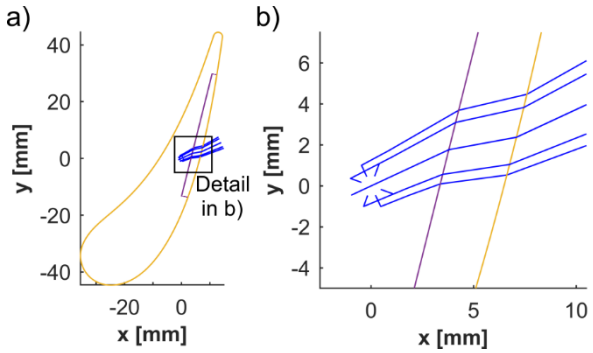


**Figure 3: Example enclosure application. a) Vane profile with the laser beam refracted through an enclosure window, b) detailed view of refraction through the window.**

even though most light is refracted through, a small percentage will always be lost as a weak reflection). $T_{rs}$ is computed using the values of transmissivity for each individual lens, as defined in the inputs.

The power density is an important parameter that is also computed at input and output. Two different power densities are computed for both cases: the Power Density Average (PDA), which takes into account the full mesh, and the Power Density Maximum (PDM), which takes into account only the core region of the beam, *i.e.* the mesh points with a value equal to unity on the Gaussian-weighted distribution. The coordinates of these points are identified for both input and output and used to calculate the required areas: areas of the full beam at input and output ($A^b_{input}$ and $A^b_{output}$) and areas of the beam core, also at input and output ($A^c_{input}$ and $A^c_{output}$). The power of the beam core at input and output ($P^c_{input}$ and $P^c_{output}$) are computed the same way (see Equations (4) and (5)) as $P^b_{input}$ and $P^b_{output}$, where $J^c$ and $K^c$ are the groups of points of the mesh corresponding to the core at input and output, respectively.

$$P^c_{input} = \frac{\sum_{j^c=1}^{J^c} A_{j^c}}{\sum_{i=1}^{I} G_i A_i} P_{beam} \qquad \textbf{(4)}$$

$$P^c_{output} = \frac{\sum_{k^c=1}^{K^c} A_{k^c}}{\sum_{i=1}^{I} G_i A_i} P_{beam} T_{rs} \qquad \textbf{(5)}$$

The power densities at the input and output are given by Equations (6) to (9).

$$\mathrm{PDA}_{input} = \frac{P^b_{input}}{A^b_{input}} \qquad \textbf{(6)} \qquad \mathrm{PDM}_{input} = \frac{P^c_{input}}{A^c_{input}} \qquad \textbf{(7)}$$

$$\mathrm{PDA}_{output} = \frac{P^b_{output}}{A^b_{output}} \qquad \textbf{(8)} \qquad \mathrm{PDM}_{output} = \frac{P^c_{output}}{A^c_{output}} \qquad \textbf{(9)}$$

The power densities can be useful in determining if a lens or coating is likely to fail under a certain input beam. Likewise, the power density at the output can be used to determine if there is enough power per unit of area for the desired application. In PIV, for instance, it is important to have enough laser power to illuminate particles introduced in the flow. If a laser beam is diverged into a larger area, the power density will be lower, thus affecting the overall performance of the PIV system.

## 3 MATHEMATICAL MODELLING

The input, the laser beam, is defined as a discretised array of beam rays, as described in Section 2.2. These rays then pass through a series of bi-concave and bi-convex lenses, spherical lenses, prisms, mirrors or even reflective surfaces with a conical or a spherical shape, each defined by Control Surfaces that are the borders between two mediums with different refractive indices.

The first step at each CS is to compute the coordinates of the intersection of each ray with the lens geometry. The second step is to compute the vector **N** normal to the CS at each intersection point. The intersection point and **N**, calculated for each ray at each control surface, are used to generate a temporary *x'y'z'* coordinate system with origin at the intersection point and the *z'* axis coincident with **N**.

The previous point in each ray is translated and rotated into its new associated local reference frame. This coordinate transformation is necessary in order to simplify the computation of the resultant laser path at each CS. Figure 4 shows the behaviour of the laser in the local reference frame. The azimuthal angle $\beta_{in}$ and polar angle $\alpha_{in}$ are computed, as shown in Figure 4a. There are two possible outcomes: the laser ray will either be refracted or experience total internal reflection (TIR). The angle of refraction can be calculated using Snell's Law (Equation (10)).

$$\alpha_{refracted} = sin^{-1}\left(\frac{n_1}{n_2}\sin(\alpha_{in})\right) \qquad \textbf{(10)}$$

Thus, the polar angle $\alpha_{out}$ can be calculated from $\alpha_{refracted}$ by $\alpha_{out} = \pi - \alpha_{refracted}$ (Figure 4b). The output azimuthal angle is simply given by: $\beta_{out} = \pi + \beta_{in}$.

For values of $\alpha_{in}$ above the critical angle $\alpha_{critical}$, given by $\alpha_{critical} = \arcsin(n_2/n_1)$, the laser ray will experience TIR. As such, $\beta_{out}$ will be the same as for the refracted case, but $\alpha_{out}$ will be equal to $\alpha_{in}$ (Figure 4c).

These calculations are repeated for each ray at each CS by taking the geometry chosen in the inputs and the ray vectors computed at the previous CS. Therefore, the number of points used to discretize the beam has a significant effect on computation time. An example calculation is carried out in Appendix I.

## 4 EXAMPLE BORESCOPE: DESIGN & MANUFACTURE

To demonstrate the versatility of the design tool as part of an iterative design process it will be applied to the design of a borescope for volumetric velocimetry inside a rotating turbomachinery rig. Since this is a technique that requires the illumination of a volume, the input laser beam must be shaped into a cone sufficiently large to cover the region of interest. Two further requirements are the employment of commercially available lenses and a maximum borescope diameter of 6mm. The input beam supplied by the laser head has a diameter of 6 mm (the beam is collimated down to 3mm after exiting the laser head). The laser has a power of 200 mJ per pulse with a 10 ns pulse width.

For the particular application of this borescope, it is desirable that the output laser rays have a direction vector with a non-negative *z* component. Since the borescope will be used to illuminate wall flows, a ray with a negative *z* component would hit the wall at an angle likely to cause reflections that obscure the camera and create noise.

The design was iterated through three stages, see Figure 5. The input details on each optical element for all designs, along with output power and power density are listed in Table 2. For all optical elements, it is assumed that 3 % of the laser power is lost through unwanted reflections.

Design 1 is comprised of two plano-cylindrical lenses positioned upstream of a prism. The two lenses and prism are among the smallest commercially available and all optics are N-BK7 without any coatings. Even though it would be possible to apply an anti-reflective coating, which would ensure less laser power was lost through the borescope, this could easily pose a problem due to the much lower laser damage threshold (LDT) of coatings when compared to a substrate material's LDT. This is particularly noteworthy in an application employing high laser power.

The two plano-cylindrical lenses used have different radii as it is beneficial (although not mandatory) to spread the laser power more in the *xy* plane that in the *xz* plane. This requirement is related to the volumetric velocimetry technique used in this paper. This experimental method is capable of measuring within a volume of 50 x 50 x 20 $mm^3$, where the 20 mm dimension corresponds to the depth. Hence, an elliptical cone is desirable to achieve the 50 x 20 $mm^2$ cross-section with maximum power. Since the 2.02 mm lens

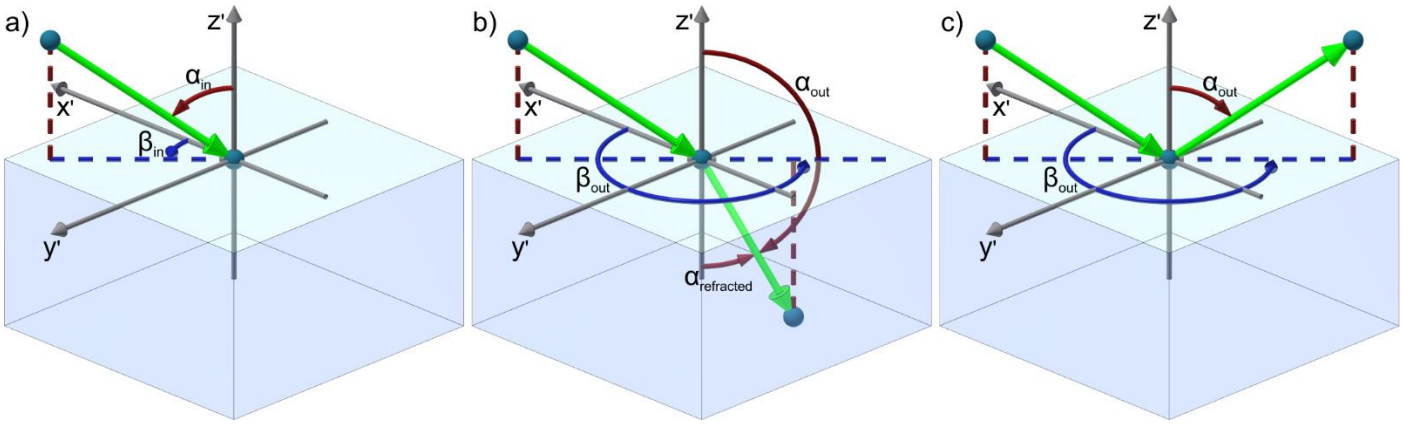


**Figure 4: Behaviour of a beam ray at the control surface of an optical element: (a) a generic input ray, (b) a refracted ray at the CS, (c) a reflected ray at the CS.**

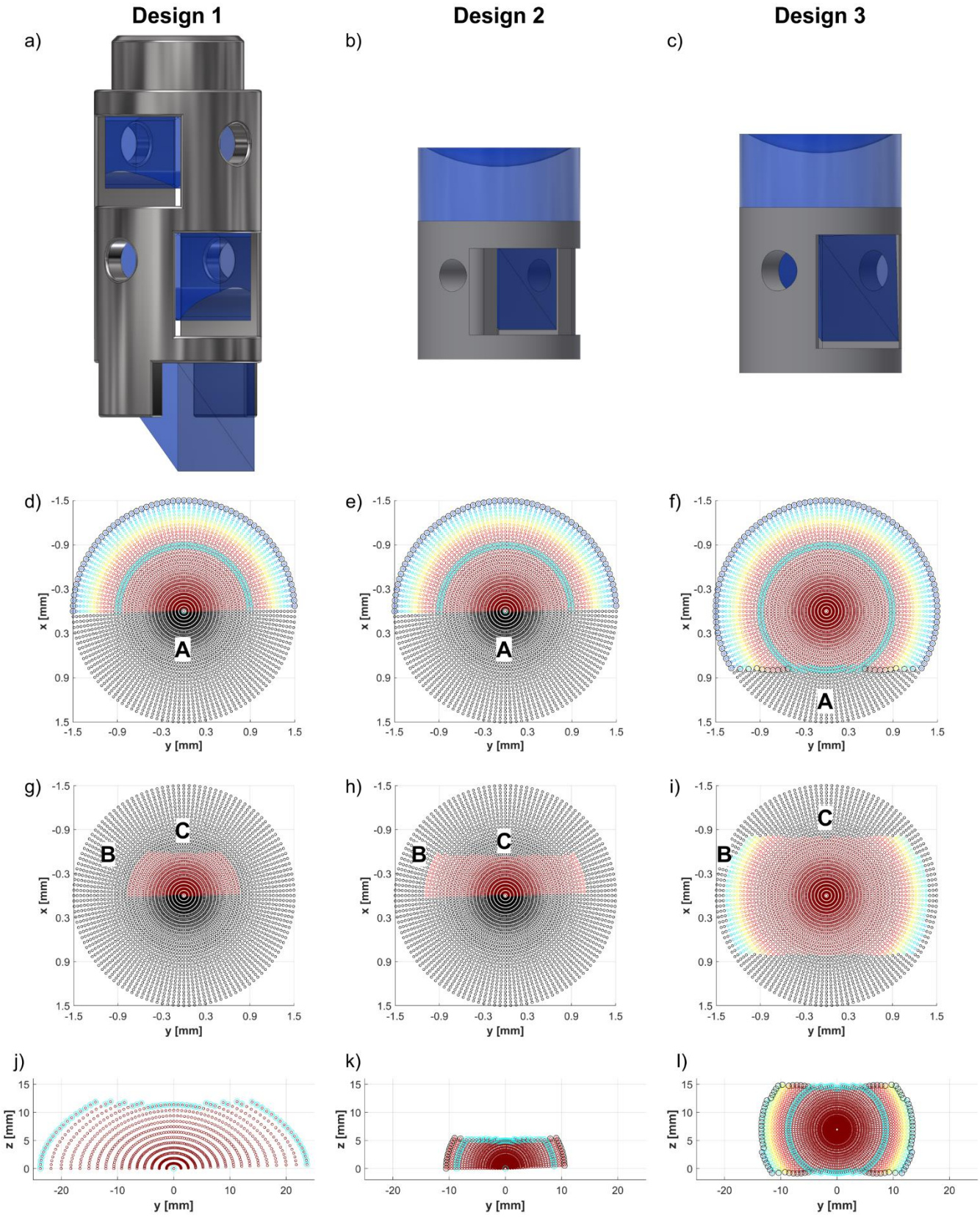


**Figure 5: Borescope Designs: a) to c) CAD representations; d) to f) input beam; g) to i) useful portion of the input beam and j) to l) beam cross-section at a distance equal to 100mm. Designs 1, 2 and 3 are left, centre and right, respectively.**

will diverge the beam significantly more, it was placed closest to the prism, *i.e.* as upstream lens 1.

The cross-section of the input laser beam is shown in Figure 5d. The beam itself has a 3 mm diameter. However, half the beam has been clipped off at the input in order to make sure the output beam has a direction vector with a non-negative *z* component. In addition, more sections of the beam are clearly lost through the borescope. These are identified by

letters B and C in Figure 5g. Region B corresponds to overexpansion of the beam going through the plano-cylindrical lenses with small radii. These parts of the beam are hitting the inner walls of the borescope. The resulting beam cross-section at a distance of 100 mm is shown in Figure 5j.

Region C is a part of the beam that reaches the rectangular face of the prism but does not experience TIR and is instead refracted out of the borescope. This is a problem that typically does not affect borescopes designed to create laser sheets but can occur for volumes. For laser sheets, as the beam is only expanded in the *yz* plane, the angle between an incident ray and the local normal is always equal to or larger than 45 degrees. For a laser volume, which is also expanded in the *xz* plane, this is not always the case, see Figure 6. This figure shows the beam behaviour for two different materials: N-BK7 and fused silica. For the incident ray in the centre, the angle between the ray and the local normal is 45 degrees, resulting in a reflected beam for both materials. The ray shown on the right has an even higher angle with respect to the local normal and will therefore be reflected as well. However, the ray on the left has a smaller angle with respect to the local normal. For fused silica, this is below the minimum angle for TIR and the ray is therefore refracted. N-BK7 has a higher index of refraction and is therefore more appropriate to ensure TIR takes place. As shown in Figure 6, with N-BK7 the laser ray is still reflected. Nevertheless, for Design 1, even using N-BK7 a large portion of the beam is still lost in region C (see Figure 5g) because the plano-cylindrical lenses have very small radii and create a strong beam divergence angle.

Even though the resulting cross-section at a 100.0 mm distance has a very satisfactory area (about 40x10 $mm^2$), the output power is very low, with a very small useful input area (Figure 5g). Half the power is lost as the beam is clipped off at the input and the output power is only 49.74 mJ. One way to increase the power output for this design would be to collimate the beam into a smaller diameter. However, tests with these N-BK7 lenses have shown they are not able to withstand a very high laser power density and display laser induced damage when smaller beam diameters are used.

Design 2 seeks to avoid the issues of laser induced damage due to high laser power density through using only fused silica lenses. The two plano-cylindrical lenses were replaced by a single plano-spherical lens. The prism used is fused silica, but with a side length of only 3 mm (4 mm prisms in fused silica are not commercially available). The borescope boss for housing the lenses is now protected from the outside, with only the front face of the prism exposed so as to protect the lenses from the freestream flow and its contaminants (the flow is seeded with oil particles).

As before, the beam was clipped off at the input (see figure 5e). Region B (Figure 5h) is considerably smaller since the radius on the plano-spherical lens is significantly larger than the radii on the plano-cylindrical lenses used in Design 1 (see Table 2). The result is a smaller beam divergence angle. However, Region C is clearly more pronounced due to the lower index of refraction of the fused silica prism. Figure 5k shows the output cross-section, where it is visible that the resulting beam has a thickness of only 5mm at a distance of 100 mm from the borescope itself. The resulting cross-

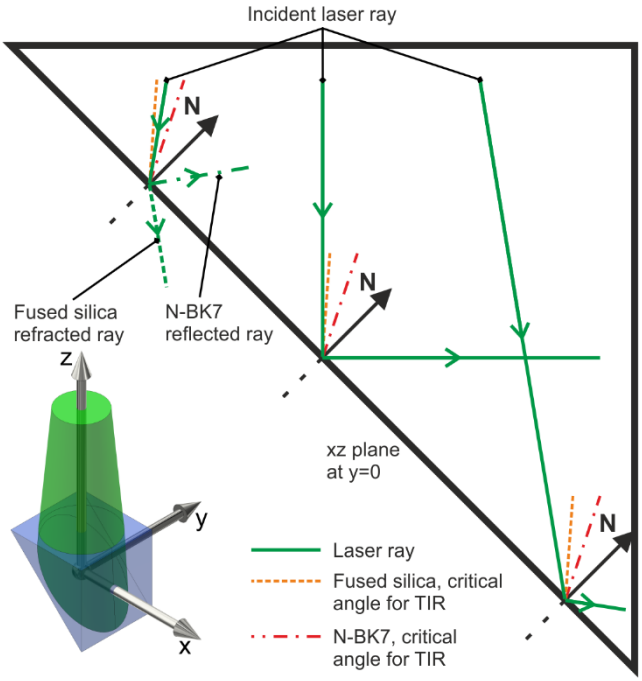


**Figure 6: Refraction or TIR for an expanding laser beam discretized into three example rays for a prism of N-BK7 and fused silica.**

sectional area of about 20x5 $mm^2$ is significantly smaller than Design 1. The output power is marginally larger and due to the smaller area the power density is significantly higher (see Table 2). This can be beneficial for optical measurements as power density will be proportional to signal-to-noise ratio. Since the output area is not large enough for the current volumetric velocimetry application, this design was improved to create Design 3.

Design 3 employs the same plano-spherical fused silica lens as Design 2. The main difference is the use of a tilted prism pointing upwards. With the prism tilted, the issue of lost power through refraction (region C) becomes more pronounced. As such, an N-BK7 prism was employed, with a 4mm leg length. Since it was found that N-BK7 prisms were much more prone to laser induced damage than fused silica the beam power was kept at 110 mJ in order to avoid power density issues. As the prism was tilted only a small portion of the input beam had to be clipped off in order to prevent an incidence angle between the laser beam and the wall at the output (see figure 5f). As a result more power is introduced into the borescope despite using the laser at a lower power level (110 mJ), see Table 2.

Region B is smaller than in Design 2 (see figure 5i), as the prism is larger and can therefore accept a larger incoming beam. Region C is also smaller than in Design 1 (as the divergence angle of the beam is smaller) and in Design 2 (N-BK7 has a higher index of refraction), despite the tilt angle of the prism. The resulting cross-section (see figure 5l) has an area of 20x14 $mm^2$, with a power output of 85.6 mJ (Table 2), significantly higher than previous designs. As this borescope design delivers a significant amount of power into the measurement region with a large enough area and no downward pointing rays, the design was chosen for the experiments described in the following section. The full 3D prediction of the laser path for Design 3 is shown in Figure

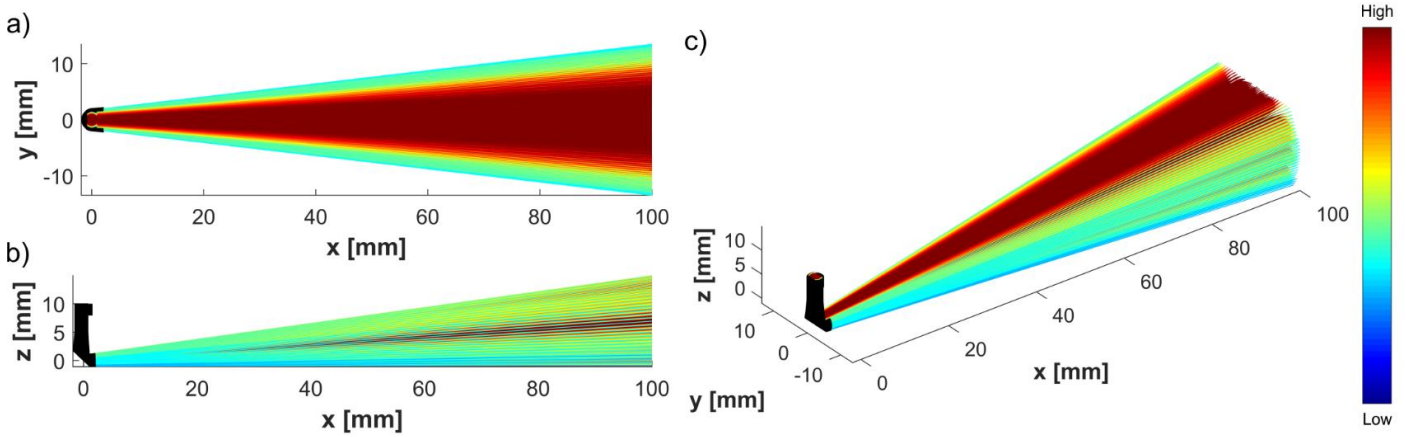


**Figure 7: Laser beam path for Borescope Design 3: a) top view (*xy*), b) lateral view (*xz*) and c) 3D view.**

7c. Figure 7a shows the spread of beam in the *xy* plane, whereas Figure 7b shows the *xz* view, where it is clear that the no beam rays are aimed into the wall, *i.e.* the lower bound rays travel parallel to the wall.

The borescope bosses shown in Figure 5a to 5c were 3D-printed in nylon infused with aluminium by Selective Laser Sintering (SLS). A small clearance is allowed for mounting all the optical elements into the borescope with NOA61 glue, especially suited for optics applications. NOA61 is capable of withstanding high temperatures and has a high transmissivity across the visible light spectrum. This clearance also allows for thermal expansion of the lenses. An assembly jig was designed and built in-house for assembly. The jig includes a class II visible laser to allow evaluation of the resulting beam as the lenses are added to the borescope boss.

## 5 EXAMPLE APPLICATION: VOLUMETRIC VELOCIMETRY

The volumetric velocimetry measurements were conducted in a stationary turbomachinery rig designed for studying film cooling with novel optical techniques such as VV and PLIF. This rig was already used successfully for conducting volumetric velocimetry measurements using direct laser input (see Carvalho Figueiredo *et al.* [12]). These measurements concerned the effect of momentum flux ratio on film cooling jets. As such, it is ideal for comparing direct laser entry with the new borescope design, Design 3.

The test section of the wind tunnel is shown in Figure 8. The laser cone used in the direct-entry measurements is shown in blue. The film cooling holes are shown in the back plate, with a borosilicate window for camera access in the front face of the wind tunnel.

The laser was guided into the borescope through a small sub-assembly attached to the front face of the wind tunnel test section. The laser beam, shown in the bottom left of Figure 8 is first reflected 90 degrees by a fused silica prism into the borescope tube. This mirror is mounted on a kinematic mount in order to control the alignment of the laser beam into the borescope tube. The borescope is introduced into the wind tunnel at a point 100 mm downstream of the film cooling holes and placed such that the resulting laser cone from the borescope (see Figure 7) travels parallel to the wall. The centre of the borescope cone is aligned with the central film cooling hole. In order to illuminate the region of interest close to the wall the borescope is partly inserted into a recess on the opposite wall, as shown in Figure 9.

Volumetric velocimetry is an increasingly relevant measurement technique in fluid dynamics research. A review on the different volumetric velocimetry methods can be found in [16]. The VV technique used (known as Defocusing PIV) requires the use of three cameras to capture the flow. Tracers are introduced in the flow and illuminated by the laser beam, introduced here by the borescope. The technique allows for measurements in a volume (3D) of the three components of velocity of the flow (3C), by making use of the relative position of the cameras, calibrated beforehand. For each capture the cameras record two frames, separated by a known time-step $\Delta t$ (3.5 µs was employed in this experimental campaign). Each frame is illuminated by an individual laser pulse. The technique aims to identify the same tracer particle in the two frames, from which the 3D displacement of the particles can be determined. The velocity is then computed using the known time-step, $\Delta t$. The instantaneous captures of the flow are then averaged into a single time-averaged result. A detailed description of the measurement principle is presented in Carvalho Figueiredo *et al.* [12]. Other

**Table 2: Design inputs and program outputs.**

| *Parameter* | *Design 1* | *Design 2* | *Design 3* |
|---|---|---|---|
| **Upstream lens 2 (lz2)** | plano-cylindrical (y-axis) concave | - | - |
| **lz2 material** | N-BK7 | | |
| **lz2 radius [mm]** | 2.99 | | |
| **Δz2 [mm]** | 10.1 | | |
| **Upstream lens 1 (lz1)** | plano-cylindrical (x-axis) concave | plano-spherical concave | plano-spherical concave |
| **lz1 material** | N-BK7 | fused silica | fused silica |
| **lz1 radius [mm]** | 2.02 | 5.5 | 5.5 |
| **Δz1 [mm]** | 5.8 | 3.5 | 4.0 |
| **$l_{prism}$[mm]** | 4.0 | 3.0 | 4.0 |
| **Prism material** | N-BK7 | fused silica | N-BK7 |
| **Prism angle [deg]** | 45.0 | 45.0 | 43.0 |
| **$P_{beam}$ [mJ]** | 200 | 200 | 110 |
| **$P_{input}$ [mJ]** | 100 | 100 | 101.6 |
| **$PDA_{input}$ [J/cm$^2$]** | 2.88 | 2.88 | 1.75 |
| **$PDM_{input}$ [J/cm$^2$]** | 5.74 | 5.74 | 3.14 |
| **$P_{output}$ [mJ]** | **49.74** | **59.35** | **85.60** |
| **$PDA_{output}$ [J/cm$^2$]** | 0.01 | 0.06 | 0.02 |
| **$PDM_{output}$ [J/cm$^2$]** | 0.01 | 0.07 | 0.03 |

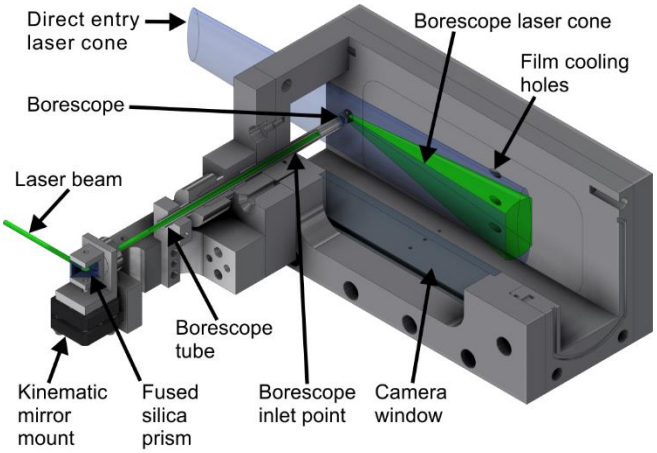


**Figure 8: Test section with different laser inputs.**

applications and work on development and optimization can be found in [13-15].

The laser delivery method is the only difference between the present and past experiments. The use of a borescope increases the complexity of the measurements as VV requires high laser power density.

A film cooling hole momentum flux ratio (IR) of 6.5 was chosen for the comparison. Film cooling is typically introduced using cylindrical or shaped holes and the interaction of the mainstream flow and coolant flow produce three-dimensional flow structures. These structures were described by Fric and Roshko [17] (see Figure 10) and Andreopoulos and Rodi [18]: a jet penetrating into the freestream and four vortex structures, a counter-rotating vortex pair (or kidney vortex), jet shear-layer vortices, wake vortices and horseshoe vortices. At high injection rates the impulse of the jet on the crossflow creates the counter-rotating vortex pair which dominates the jet structure in the far field, modifying its cross-section into a kidney-shaped form. The kidney vortex structure is well pronounced for IR=6.5 and therefore serves as an effective validation case.

The three film cooling holes shown in Figure 8 have a diameter (*D*) of 4mm, a length-to-diameter ratio of 2.8 and a pitch-to-diameter ratio equal to 4. The hole angle $\alpha_h$ is 30 degrees and the Mach number (M) of the freestream main flow is 0.3. The density ratio (DR) between the two flows is approximately 1.5, as air is used as the main gas path and $CO_2$ is used as the coolant.

The raw images of the particles showed that, as expected, due to the lower laser power the illumination was weaker for the borescope than the direct entry approach. This weaker illumination will make particle identification substantially more difficult as the difference between particle intensity and background intensity is smaller resulting in a reduced number of valid particles detected in each image set. As a result during the subsequent triplet and vector identification stages a lower number of triplets and therefore velocity vectors will be identified. Conversely, the number of false vectors due to reflections on the wall will remain similar. The combination of reduced valid vectors with constant noise vectors yields a lower signal-to-noise ratio. The number of velocity vectors identified can be compensated for by taking more captures of the flow. As such, 2500 captures were taken for the borescope case, whereas for the direct-entry case only 500 captures were

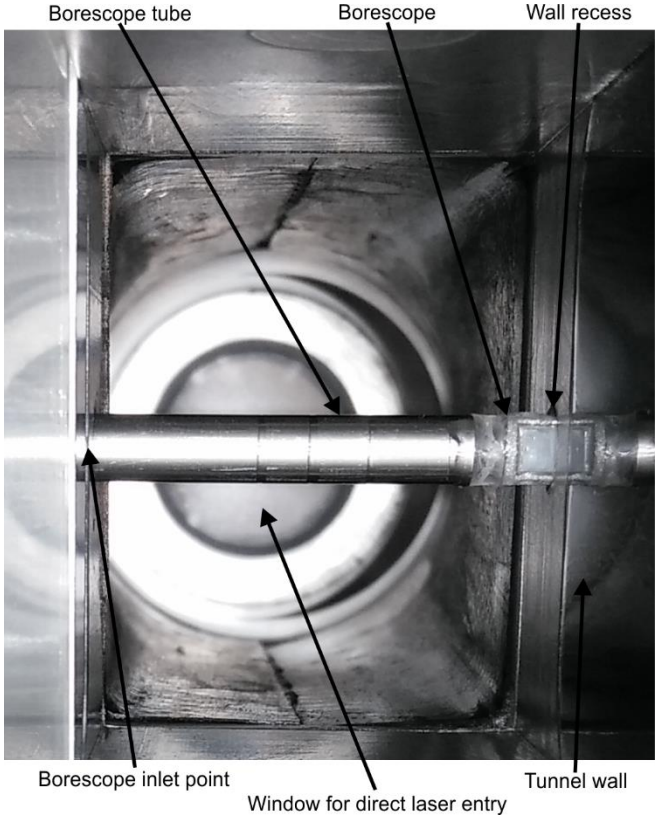


**Figure 9: Borescope Design 3 *in-situ*.**

taken. A global filter was also employed in order to filter out false particles arising from reflections off the wall.

The results of VV with the borescope application are shown in Figure 11 (right), compared with the direct-entry measurements (left). Figure 11 a) and b) show an isosurface of velocity with $u/U_\infty = 1.05$ for a range of $x/D$ from 2 to 8. Figure 11 c) and d) show a contour of the *u* component of velocity. Despite the lower laser power, it was still possible to capture the film cooling jet produced by the high momentum flux ratio, particularly the dominant *u* component, as shown by the isosurface. The isosurface shows the same kidney vortex shape observed for the direct-entry case, created by the mixing mechanisms due to the impulse of the jet on the crossflow. The kidney vortex shape is the dominant feature observed in a film cooling jet, as shown in Figure 10 (Fric and Roshko [17]).

Figure 11 c) and d) show the curved centreline of the jet. As expected the effect of lower laser power is noticeable with

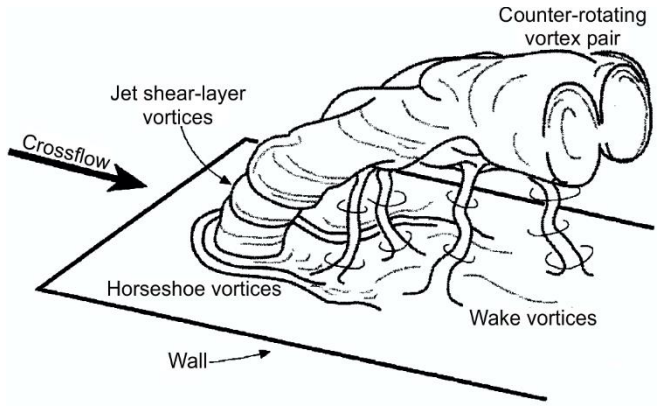


**Figure 10: Film cooling flow structures according to Fric and Roshko [17].**

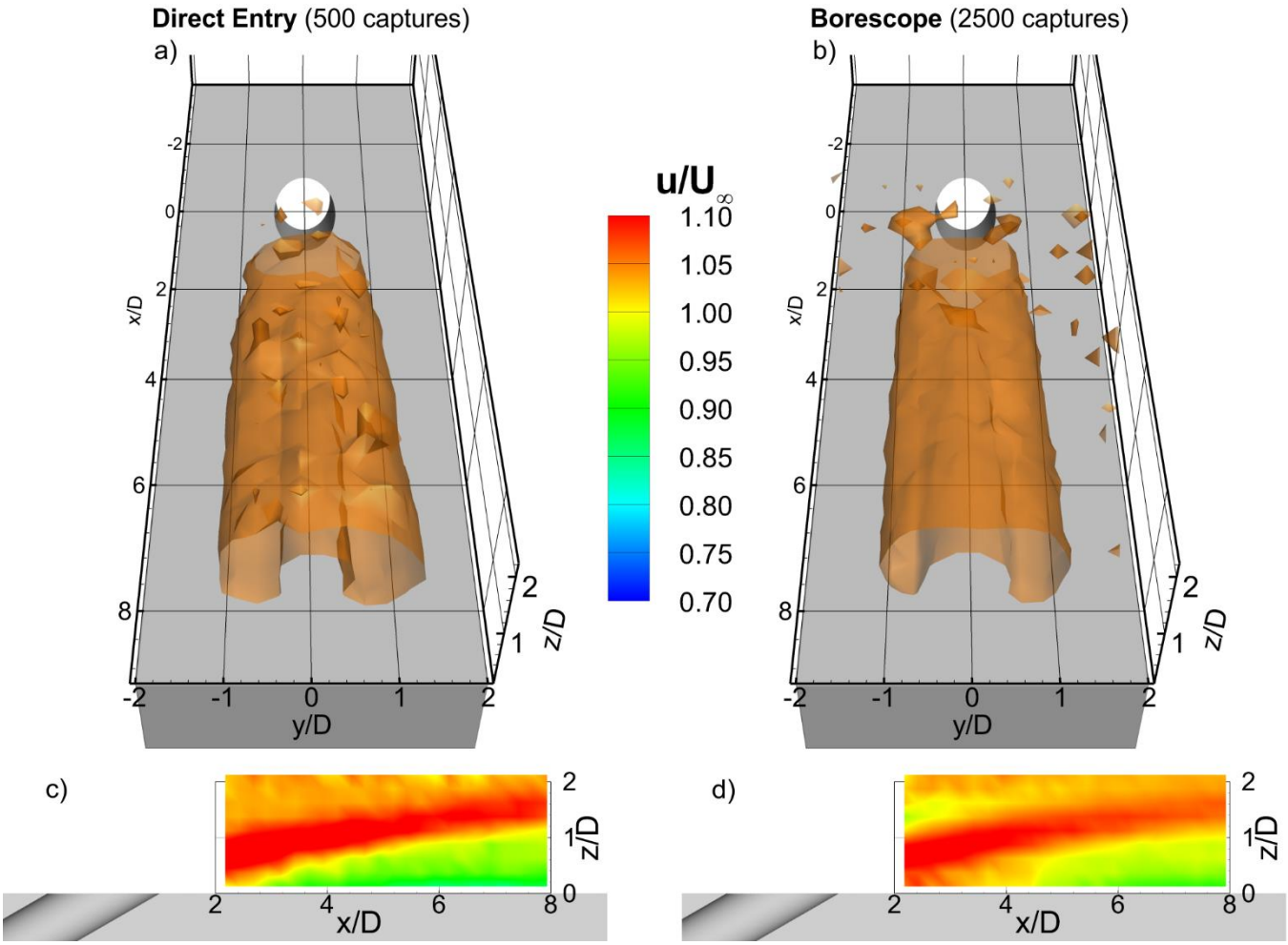


**Figure 11: VV application: Isosurface ($u/U_\infty$=1.05) for Direct Entry (a) and for Borescope (b), $u/U_\infty$ contour at y/D=0 for Direct Entry (c) and for Borescope (d).**

less quality in the borescope results than in the direct laser entry case. Nevertheless, the behaviour of the jet was captured, with evident detachment of the jet off the wall and a curving trajectory as the jet interacts with the main flow.

This flow is also characterized by very small $v$ and $w$ components ($< 0.1U_\infty$) which could not be captured fully with the lower laser power used in the borescope. The use of more exotic materials for the lenses would be required in order to allow more laser power to travel through the borescope and into the region of interest without laser induced damage. In particular for the prism, whereas N-BK7 provides the best angle range for TIR, it is also more prone to fail under high laser power. The use of a material such as sapphire, which has both a high index of refraction and a high laser damage threshold would be ideal. However, there is limited commercial availability of sapphire optical elements, partly due to the higher cost of the substrate but also due to the hardness of the material, which makes polishing difficult.

From the measurements it was also possible to conclude that there are a minimum and a maximum distances that limit the region where good data can be obtained. The maximum distance is related to the decreasing laser power density as the cone expands. For a flow seeded with oil droplets, the amount of actual power also decreases as the beam travels through a medium populated with particles.

The minimum distance away from the borescope is also related to the laser power density. As all laser power is concentrated in a very small region the illuminated particles in a heavily seeded flow can actually produce a signal that is too strong (particles would appear overlapped). However, this would not usually be an issue since the volume illuminated near the borescope is too small to be employed as the region of interest for most applications.

Although the lenses on the borescope were protected from the seeding tracers in the flow by the borescope boss, the front face of the prism, shown in Figure 9, was inevitably exposed in order to allow the beam to travel through and illuminate the measurement region. With time this surface would be contaminated with particles from the flow, with an adverse effect on the amount of laser power reaching the measurement region. Cleaning of the borescope was necessary once the loss in laser power impacted the quality of the data acquired.

This section illustrates the potential for employing borescopes in wind tunnels with restricted access, even for high power applications like volumetric velocimetry. In spite of the limitations on laser power it was possible to successfully illuminate a volume using a borescope, whereas all previous borescopes applications have considered lower power single planes.

## 6 CONCLUSIONS

A design tool was developed to predict the laser path and power distribution from a borescope. The program can be employed to design borescopes for optical measurements in wind tunnels with restricted access. The code structure and mathematical modelling of the optics and laser input are also described, along with tools provided for assessing the quality of the design.

The program was applied to the iterative design of a borescope for volumetric velocimetry measurements inside turbomachinery. Three different designs were developed and evaluated as to the resulting laser beam and available power. Several issues were identified during the design phase, helping drive subsequent borescope designs. In particular, it was found and demonstrated using the program that a prism with a high index of refraction can be highly beneficial for this application. Furthermore the laser power density was limited by the damage threshold of N-BK7 optics and limited commercial availability of fused silica. Nevertheless the higher index of refraction for N-BK7 justified its use for the prism because it enables a higher angle range for total internal reflection.

The final design was manufactured in-house and tested in a turbomachinery wind tunnel facility in the study of film cooling through volumetric velocimetry. Despite the lower laser power, it was possible to capture the three-dimensional flow features of the film cooling jet as it interacted with the flow. The results were compared to previous measurements taken with a direct laser illumination in order to validate the film cooling jet measurements obtained with the borescope, with very good agreement. This demonstrates the importance of a versatile and robust borescope design tool for quick design iterations. The program is available as supplementary material to enable future research in the application of optical laser measurements in highly constrained environments.


## ACKNOWLEDGMENTS

The authors would like to thank Andrew Langley, Terrence Warder, Nigel Gillard and all other technicians involved in the manufacture and assembly of the film cooling rig for these experiments. The research described here was supported by the *Engineering and Physical Sciences Research Council* (EPSRC) through grant number EP/M026345/1. The VV system is part of the *Versatile Fluid Measurement System* (VFMS), acquired through the EPSRC Strategic Equipment Panel (grant number EP/K040391/1). Data access: Due to confidentiality agreements with research collaborators, supporting data can only be made available to bona fide researchers subject to a nondisclosure agreement. Details of how to request access are available at the University of Bath data archive website[2].

## FUNDING DATA

- Engineering and Physical Sciences Research Council (EP/ M026345/1 and EP/K040391/1).


## NOMENCLATURE

| | |
|---|---|
| $a$ | speed of sound |
| $A$ | Area |
| CS | Control Surface |
| $D$ | hole diameter |
| $D_{beam}$ | beam diameter |
| DR | density ratio $\left(\mathrm{DR} = \frac{\rho_c}{\rho_m}\right)$ |
| $g$ | hole pitch |
| $G$ | value in Gaussian-weighted distribution of power |
| $i$ | individual point in group $I$ |
| $I$ | group of points in the MATLAB mesh |
| IR | momentum flux ratio $\left(\mathrm{IR} = \frac{\rho_c U_c^2}{\rho_m U_m^2}\right)$ |
| $j$ | individual point in group $J$ |
| $J$ | group of points in the MATLAB mesh after the input |
| $k$ | individual point in group $K$ |
| $K$ | group of points in the MATLAB mesh after the output |
| $l$ | hole length |
| $l_{prism}$ | prism leg length |
| lz1 | Upstream Lens 1 |
| lz2 | Upstream Lens 2 |
| M | Mach number $\left(\mathrm{M} = \frac{U_\infty}{a}\right)$ |
| $n$ | index of refraction of the medium |
| $N_c$ | number of circles or ellipses in the mesh |
| $N_p$ | number of points in each circle or ellipses of the mesh |
| **N** | Vector normal to a surface |
| $P$ | Laser power |
| PDA | Power Density Average |
| PDM | Power Density Maximum |
| $R_y$ | rotation matrix about $y$ |
| $R_z$ | rotation matrix about $z$ |
| $T$ | translation matrix |
| $T_{rs}$ | overall transmissivity of the borescope lenses |
| TIR | Total Internal Reflection |
| $u$ | streamwise component of velocity |
| $U$ | velocity magnitude |
| $U_\infty$ | freestream velocity |
| $V$ | volume |
| **V** | velocity vector |
| $x$ | streamwise coordinate |
| $y$ | lateral coordinate |
| $z$ | vertical coordinate |
| $xyz$ | film cooling rig reference frame |
| $xyz$ | borescope reference frame |
| $x'y'z'$ | local reference frame at a control surface |
| $\alpha_h$ | hole angle |
| $\alpha$ | polar angle of beam ray |
| $\beta$ | azimuthal angle of beam ray |
| $\Delta t$ | laser pulse time-step |
| $\theta$ | rotation angle in $R_z$ |
| $\rho$ | density |
| $\phi$ | rotation angle in $R_y$ |

### Subscripts

| | |
|---|---|
| *1* | first medium |
| 2 | second medium |
| *beam* | laser beam |
| *c* | coolant flow |

[2] http://dx.doi.org/10.15125/BATH-00116

*d* dummy point
*in* inbound beam ray
*input* at the borescope input
*m* main flow
*out* outbound beam ray
*output* at the borescope ouput
*refracted* refracted beam ray

**Superscripts**
*b* full area of the laser beam
*c* core area of the laser beam

## REFERENCES


[1] J. Woisetschläger, E. Göttlich, Recent Applications of Particle Image Velocimetry to Flow Research in Thermal Turbomachinery, Particle Image Velocimetry, Springer2007, pp. 311-331.

[2] N. Balzani, F. Scarano, M. Riethmuller, F. Breugelmans, Experimental investigation of the blade-to-blade flow in a compressor rotor by digital particle image velocimetry, ASME Turbo Expo 2000: Power for Land, Sea, and Air, American Society of Mechanical Engineers2000, pp. V004T004A025-V004T004A025.

[3] E. Göttlich, J. Woisetschläger, P. Pieringer, B. Hampel, F. Heitmeir, Investigation of vortex shedding and wake-wake interaction in a transonic turbine stage using laser-doppler-velocimetry and particle-image-velocimetry, Journal of turbomachinery, 128 (2006) 178-187.

[4] B. Liu, X. Yu, H. Liu, H. Jiang, H. Yuan, Y. Xu, Application of SPIV in turbomachinery, Experiments in Fluids, 40 (2006) 621-642.

[5] M.P. Wernet, Application of DPIV to study both steady state and transient turbomachinery flows, Optics & Laser Technology, 32 (2000) 497-525.

[6] W. Copenhaver, J. Estevadeordal, S. Gogineni, S. Gorrell, L. Goss, DPIV study of near-stall wake-rotor interactions in a transonic compressor, Experiments in fluids, 33 (2002) 899-908.

[7] P.J. Bryanston-Cross, C.E. Towers, T.R. Judge, D.P. Towers, S.P. Harasgama, S.T. Hopwood, The application of particle image velocimetry (PIV) in a short duration transonic annular turbine cascade, ASME 1991 International Gas Turbine and Aeroengine Congress and Exposition, American Society of Mechanical Engineers1991, pp. V001T001A078-V001T001A078.

[8] K.S. Chana, N. Healey, P.J. Bryanston-Cross, Particle Image Velocimetry Measurements from the Stator-Rotor Interaction Region of a High Pressure Transonic Turbine Stage at the DERA Isentropic Light Piston Facility, AGARD Conference Proceedings 598, AGARD-CP-598, (1998).

[9] T. Geis, G. Rottenkolber, M. Dittmann, B. Richter, K. Dullenkopf, S. Wittig, Endoscopic PIV-measurements in an enclosed rotor-stator system with pre-swirled cooling air, Proceedings of the 11th International Symposium on Applications of Laser Techniques to Fluid Mechanics2002, pp. 8-11.

[10] M. Kegalj, H.-P. Schiffer, Endoscopic PIV measurements in a low pressure turbine rig, Experiments in fluids, 47 (2009) 689.

[11] Y.-C. Chow, O. Uzol, J. Katz, Flow non-uniformities and turbulent "hot spots" due to wake-blade and wake-wake interactions in a multistage turbomachine, ASME Turbo Expo 2002: Power for Land, Sea, and Air, American Society of Mechanical Engineers2002, pp. 1215-1227.

[12] A.J. Carvalho Figueiredo, R. Jones, O.J. Pountney, J.A. Scobie, G.D. Lock, C.M. Sangan, D.J. Cleaver, Volumetric Velocimetry Measurements of Film Cooling Jets, Journal of Engineering for Gas Turbines and Power, 141 (2018) 031021-031021-031013.

[13] D. Cleaver, Z. Wang, I. Gursul, Oscillating flexible wings at low Reynolds numbers, 51st AIAA Aerospace Sciences Meeting, University of Bath2013.

[14] D.E. Calderon, Z. Wang, I. Gursul, M.R. Visbal, Volumetric measurements and simulations of the vortex structures generated by low aspect ratio plunging wings, (2013).

[15] T. Cambonie, J.-L. Aider, Seeding optimization for instantaneous volumetric velocimetry. Application to a jet in crossflow, Optics and Lasers in Engineering, 56 (2014) 99-112.

[16] S. Discetti, F. Coletti, Volumetric velocimetry for fluid flows, Measurement Science and Technology, 29 (2018) 042001.

[17] T. Fric, A. Roshko, Vortical structure in the wake of a transverse jet, Journal of Fluid Mechanics, 279 (1994) 1-47.

[18] J. Andreopoulos, W. Rodi, Experimental investigation of jets in a crossflow, Journal of Fluid Mechanics, 138 (1984) 93-127.


## APPENDIX I

As an example, this appendix will consider the borescope design used for VV in Sections 4 and 5. This design is composed of a plano-concave spherical lens, used to create a beam cone with a circular cross-section, and a right angle prism, used to reflect the beam into the region of interest. Only one example beam ray is considered to illustrate the process, see Figure 12. The ray itself and the points at the control surfaces are shown in green.

The initial cross-section of the beam has a diameter of 3 mm. The chosen example ray has initial coordinates of $CS1 = (0.53, 0.53, 10.0)$, with a dummy point of $CS1d = (0.53, 0.53, 9.0)$, which implies a direction vector of (0,0,-1). As this design features only one lens upstream of the prism, CSs 2 and 3 are ignored (see Figure 1).

On CS4, the ray meets the spherical surface of the plano-concave lens. The intersection between the line, representing the laser ray, and the sphere, representing the spherical surface of the lens, yields the coordinates $CS4 = (0.53, 0.53, 5.05)$. The normal $\mathbf{N} = (N_x, N_y, N_z)$ to the surface at this location is given by the difference between the coordinates of the centre of the sphere $(0, 0, 10.5)$ and the coordinates of the intersection point. This results in $\mathbf{N} = (-0.53, -0.53, 5.45)$.

The normal **N** is used to compute the angles $\theta$ and $\phi$, given by $\theta = \tan^{-1}(N_y/N_x) = -135°$ (the MATLAB function *atan2*, a four-quadrant inverse tangent, is used to compute $\theta$) and $\phi = \tan^{-1}(\sqrt{N_x^2 + N_y^2}/N_z) = 7.84°$. The coordinates at the previous control surface (in this case CS1) are then calculated in a new reference frame with origin at the intersection point $CS4$ and with the axis z' coincident with **N**, using $CS1' = R_y R_z (CS1 - T)$, where $R_y$ and $R_z$ are rotation matrices (Equations (11) and (12)) and T is a translation matrix given by Equation (13).

$$R_y = \begin{bmatrix} \cos(\phi) & 0 & -\sin(\phi) & 0 \\ 0 & 1 & 0 & 0 \\ \sin(\phi) & 0 & \cos(\phi) & 0 \\ 0 & 0 & 0 & 1 \end{bmatrix} \quad \textbf{(11)}$$

$$R_z = \begin{bmatrix} \cos(\theta) & 0 & \sin(\theta) & 0 \\ -\sin(\theta) & 1 & \cos(\theta) & 0 \\ 0 & 0 & 1 & 0 \\ 0 & 0 & 0 & 1 \end{bmatrix} \quad \textbf{(12)}$$

$$T = \begin{bmatrix} CS2_x \\ CS2_y \\ CS2_z \\ 0 \end{bmatrix} \quad \textbf{(13)}$$

The $CS1' = (-0.67, 0, 4.90)$ coordinates obtained are used to compute $\alpha_{in}$ and $\beta_{in}$ (see Figure 4a), using $\alpha_{in} = \tan^{-1}\left(\sqrt{CS1'_x{}^2 + CS1'_y{}^2}/CS1'_z\right) = 7.84°$ and $\beta_{in} = \tan^{-1}(CS1'_y/CS1'_x) = 180°$. As the angle $\alpha_{in} < \alpha_{critical} = 43.20°$, this beam ray will be refracted at this CS. Snell's law is applied to yield $\alpha_{refracted} = \sin^{-1}(n_1/n_2 \sin(\alpha_{in})) = 5.36°$, which results in $\alpha_{out} = 174.64°$. As $\beta_{in} = 180°$, it follows that $\beta_{out} = 360°$.

The coordinates of the dummy point in the local reference frame for CS4 are calculated using these two angles: $CS4d' = (\sin(\alpha_{out})\cos(\beta_{out}), \sin(\alpha_{out})\sin(\beta_{out}), \cos(\alpha_{out})) = (0.093, 0.0, -0.996)$.

The coordinates of the same dummy point in the main borescope reference frame are then given by: $CS4d = (R_y R_z)^{-1} CS4d' + T = (0.56, 0.56, 4.05)$.

The normalized direction vector at CS4 is equal to $(0.03, 0.03, -1.0)$, showing that the beam is now diverging away from the *z* axis of the borescope.

Subsequent CSs are in all similar, with a first calculation of the intersection point, enabled by the direction vector obtained from the dummy point computed at the previous CS. The remaining coordinates for this beam ray example are listed in Table 3.

**Table 3: Point data for example ray.**

| *CS* | *x* | *y* | *z* | $x_d$ | $y_d$ | $z_d$ |
|---|---|---|---|---|---|---|
| **1** | 0.53 | 0.53 | 10.0 | 0.53 | 0.53 | 9.0 |
| **2-3** | | | - | | | |
| **4** | 0.53 | 0.53 | 5.05 | 0.56 | 0.56 | 4.05 |
| **5** | 0.59 | 0.59 | 3.0 | 0.64 | 0.64 | 2.0 |
| **6** | 0.64 | 0.64 | 2.02 | 0.68 | 0.67 | 1.02 |
| **7** | 0.75 | 0.72 | -0.70 | 1.75 | 0.75 | -0.67 |
| **8** | 2.02 | 0.75 | -0.66 | 3.02 | 0.80 | -0.64 |
| **9-14** | | | - | | | |
| **15** | 10.0 | 1.11 | 0.46 | | - | |

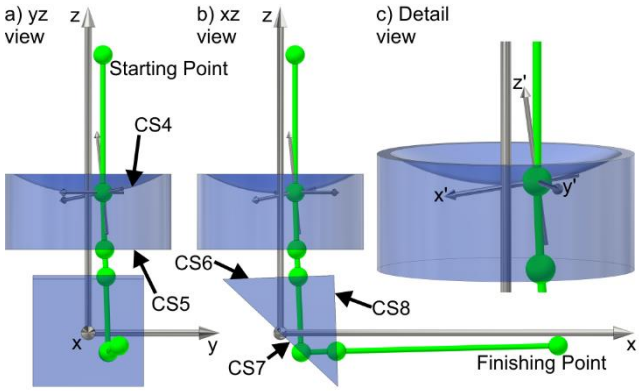


**Figure 12: Laser ray behaviour at a control surface CS: *yz* view (left), *xz* view (centre) and CS4 detail (right).**